

# Impact of Loss Mechanisms on Linear Spectra of Excitonic and Polaritonic Aggregates

Devansh Sharma and Amartya Bose<sup>a)</sup>

*Department of Chemical Sciences, Tata Institute of Fundamental Research, Mumbai 400005, India*

The presence of loss mechanisms governed by empirical time-scales affect the dynamics and spectra of systems in profound ways. However, incorporation of these effects and their interaction with the thermal dissipative environments interacting with the system prove to be challenging. We have recently developed the path integral Lindblad dynamics (PILD) method to combine numerically rigorous path integral simulations with Lindblad dynamics to account for such empirical loss mechanisms. In this work, we utilize the PILD method to study the absorption and circular dichroism spectra of chiral molecular aggregates and excitonic polaritons. We demonstrate that the effect of loss on particular states in both systems can differ not just on the basis of the symmetries of the state but also on the basis of complicated “interactions” of the system and the loss mechanism with the dissipative environments. We present probably the first numerical exploration of the CD spectrum of chiral molecular aggregates confined in a cavity. While the CD spectrum of just the excitonic aggregates itself is not amenable to simplistic understanding like the exciton chirality (EC) rule, the CD spectrum of polaritonic molecules is even more complex. Additionally, the impact of empirical loss on the polaritonic CD spectrum seems to be highly site-dependent. The impact of a lossy cavity is qualitatively different from the impact of a molecule that leaks the excitation. We explore some of those effects in depth leveraging the framework of path integral Lindblad dynamics.

## I. INTRODUCTION

Spectroscopy is one of the most basic tools for characterizing chemical systems. While absorption spectra gives an insight into the electronic structure, circular dichroism spectra provides insights into the geometry of chiral systems. These spectra are broadened due to the coupling of the eigenstates states to environment degrees of freedom which are usually thermally populated. Simulations of the exact lineshape proves to be challenging owing to the continuous manifold of environmental states participating in the dynamics. The presence of loss mechanisms in many systems additionally broadens the spectral features, which poses an additional challenge to accurate predictions of these broadened line-shapes. Methods based on wave functions such as density matrix renormalization group<sup>1–4</sup> or multiconfiguration time-dependent Hartree<sup>5</sup> and its multilayer formulation<sup>6,7</sup> have been pushing the limits of what is computationally tractable, however, they still are inadequate in describing the dynamics in the condensed phase where a continuum of environment degrees of freedom are thermally populated.

Methods that simulate the reduced density matrix (RDM) of the system overcome many of these challenges by integrating out an appropriately selected set of environment modes. This tracing over the environment makes the dynamics non-Markovian. Various approximate methods like the Bloch-Redfield master equation<sup>8,9</sup> and the Lindblad or the Gorini-Kossakowski-Sudarshan-Lindblad master equation<sup>10,11</sup> treat the bath perturba-

tively or make a Markovian approximation for the dynamics. Mixed quantum classical methods like surface hopping<sup>12,13</sup> treat the environment classically. However, the results obtained from these methods cannot be improved systematically. Feynman’s path integral approach<sup>14</sup> provides an alternate route to simulating such systems that is numerically rigorous. The environment modes are incorporated using the Feynman-Vernon influence functional.<sup>15</sup> The hierarchical equation of motion<sup>16,17</sup> (HEOM) and the quasi-adiabatic propagator path integral<sup>18,19</sup> (QuAPI) and later developments on them<sup>20–29</sup> provide lucrative ways of implementing path integral for large open quantum systems. Recent applications on large biomolecular aggregates<sup>29–32</sup> show the full power and applicability of these methods in simulating large systems.

However, it is generally difficult to incorporate loss or gain processes described by empirical time scales into numerically exact simulations. These empirical loss mechanisms are, in fact, quite ubiquitous. Consider, for example, the loss of an exciton at particular sink sites to the “special pair” in photosynthetic aggregates or the loss of photons from leaky cavities. It is not always possible to characterize such processes using proper spectral densities and harmonic baths. Use of a fictitious bath can often induce artifacts stemming from particular functional form used. While non-Hermitian descriptions can be used in some cases, the resultant dynamics is non-unitary leading to spurious effects in correlation functions and spectra. The Lindblad master equation, which maintains the unitarity of evolution, offers a lucrative alternative to these non-Hermitian descriptions in simulating such systems. Now, while the Lindblad approach is good for the lossy modes, we do not want to treat the effect of the thermal vibrations using Lind-

<sup>a)</sup>Electronic mail: [amartya.bose@tifr.res.in](mailto:amartya.bose@tifr.res.in)

blad dynamics. A combination of the fully semiclassical partial linearized density matrix<sup>33,34</sup> with Lindblad master equation has been used to study the effect of losses on the 2D electronic spectra of polaritonic aggregates by Mondal *et al.*<sup>35</sup> Recently, one of us has developed an efficient approach towards combining numerically exact QuAPI simulations, accounting for the bath effects, with the Lindblad master equation to account for such empirical loss mechanisms at no extra cost.<sup>36</sup> This path integral Lindblad dynamics (PILD) approach guarantees a positive definite dynamical map for the dynamics. Being based on QuAPI, it is able to handle arbitrary thermal environments with equal ease. In addition different loss mechanisms can be studied in parallel without having to rerun the path integral simulation. The impact of the loss of an exciton on the dynamics in the Fenna–Matthew–Olson complex was explored.<sup>36</sup>

Here we extend the PILD approach to simulate the line-shapes of linear spectra of aggregates in presence of loss and attempt to answer the natural question: how does the spectrum of a system get affected by the presence of these loss mechanisms? These losses become especially interesting in cases of excitonic molecular wires where the exciton is lost at one site, and excitonic polaritons where the cavity is known to be lossy. In Sec. II, we summarize the path integral Lindblad dynamics framework<sup>36</sup> and extend it to allow the study of linear spectra. In Sec. III, we describe the chiral molecular aggregates that are of interest. We explore the absorption and CD spectra under different loss cases. While one might be tempted to make simple generalizations about the impact of loss on the absorption and CD spectra, it seems that little can be simply stated beyond the fact that loss, in general, broadens peaks and decreases their intensities. We show that which peak is broadened and by what amount is a non-trivial problem. We come up with rules of thumb, which while still not complete, gives a better zeroth order approximate understanding of the phenomenon. We demonstrate the caveats involved by probing deeper. PILD allows for a simple incorporation of processes described by empirical timescales in rigorous numerical simulations for the first time. Finally, we end by providing some concluding remarks and future directions in Sec. IV.

## II. METHOD

Consider an open quantum system described by a system-environment decomposed Hamiltonian,

$$H = H_0 + H_{\text{env}}, \quad (1)$$

where  $H_0$  is the system Hamiltonian and  $H_{\text{env}}$  is the Hamiltonian describing the environment and its interaction with the system. For a typical exciton transport system, the system can be defined in terms of the singly excited subspace spanned by  $|j\rangle$  representing the excitation occurring on the  $j$ th molecule with all other molecules in

the ground state. The resultant Hamiltonian has the well-known Frenkel form:

$$H_0 = \sum_j \epsilon_j |j\rangle\langle j| + \sum_{jk} h_{jk} (|j\rangle\langle k| + |k\rangle\langle j|), \quad (2)$$

where  $\epsilon_j$  is the energy of the locally excited state on the  $j$ th molecule and  $h_{jk}$  is the amplitude for the excitation to hop from the  $j$ th to the  $k$ th molecule. Notice that this Hamiltonian has been expressed in the so-called first-excitation subspace. For the simulation of spectra, it will be necessary to augment the basis with the electronic ground state,  $|0\rangle$ , which has all the monomers in the ground state.

The environment includes the thermal solvent to which the system is exposed and the molecular vibrations of the system. Under linear response, these modulations can be mapped on to baths of harmonic oscillators that locally interact with a monomer,

$$H_{\text{env}} = \sum_j \sum_b \frac{p_{jb}^2}{2} + \frac{1}{2} \omega_{jb}^2 x_{jb}^2 - c_{jb} x_{jb} |j\rangle\langle j|, \quad (3)$$

where  $\omega_{jb}$  is the frequency of the  $b$ th harmonic mode that interacts with the  $j$ th molecule and  $c_{jb}$  is the corresponding coupling. The mapping of a molecular solvent onto this set of harmonic baths is done through the bath spectral density

$$J_j(\omega) = \frac{\pi}{2} \sum_b \frac{c_{jb}^2}{\omega_{jb}} \delta(\omega - \omega_{jb}). \quad (4)$$

For a molecular solvent,  $J_j(\omega)$  can be calculated using molecular dynamics simulations.<sup>37,38</sup> In addition to this environment, the system also has loss mechanisms which cannot be described in this Hamiltonian formalism. These would be incorporated using the Lindblad master equation.<sup>10,11</sup> Therefore, we need a way to simulate the reduced density matrix of the system in the presence of both the thermal environment and the Lindbladian jump operators  $L_j$ .

According to the path integral Lindblad dynamics<sup>36</sup> approach, the loss mechanisms are incorporated using a modified Nakajima-Zwanzig master equation.<sup>39,40</sup> If the initial state is uncorrelated,  $\rho(0) = \tilde{\rho}(0) \otimes \exp(-\beta H_{\text{env}})/Z$ , then the time-evolution of the reduced density matrix corresponding to the system is given by:

$$\begin{aligned} \dot{\tilde{\rho}}^{(L)}(t) = & -\frac{i}{\hbar} \mathcal{L}_0 \tilde{\rho}^{(L)}(t) + \int_0^{\tau_{\text{mem}}} \mathcal{K}(\tau) \tilde{\rho}^{(L)}(t - \tau) d\tau \\ & + \sum_j \left( L_j \tilde{\rho}^{(L)}(t) L_j^\dagger - \frac{1}{2} \{ L_j^\dagger L_j, \tilde{\rho}^{(L)}(t) \} \right) \end{aligned} \quad (5)$$

where  $\tilde{\rho}^{(L)}(t)$  is the time-evolved reduced density matrix for the open quantum system under the influence of the Lindbladian jump operators,  $\mathcal{L}_0 = [H_0, \cdot]$  is the system Liouvillian,  $\mathcal{K}$  is the memory kernel corresponding to the thermal environment, and  $\tau_{\text{mem}}$  is the memory length.

Obtaining the memory kernel,  $\mathcal{K}$ , is extremely challenging. While various ways of approximately evaluating the memory kernel exists using approximate simulations of dynamics,<sup>41,42</sup> these are not controlled approximations. We, on the other hand, use the framework of transfer tensor method (TTM),<sup>20</sup> which decomposes the dynamical maps,  $\mathcal{E}(t)$ , of the reduced system defined by  $\tilde{\rho}(t) = \mathcal{E}(t)\tilde{\rho}(0)$ , in terms of transfer tensors  $T_k$  defined as

$$T_k = \mathcal{E}(k\Delta t) - \sum_{m \geq 1} T_m \mathcal{E}((k-m)\Delta t), \quad (6)$$

such that the time evolution of the system can be expressed as

$$\tilde{\rho}(t_n) = \sum_{k=1}^L T_k \tilde{\rho}(t_{n-k}) \quad (7)$$

where  $L\Delta t = \tau_{\text{mem}}$ . These transfer tensors can now be related to the memory kernel as

$$T_k = \mathcal{E}_0(\Delta t)\delta_{k,1} + \mathcal{K}_k \Delta t^2 \quad (8)$$

where  $\mathcal{E}_0(t) = \exp(-iH_0t/\hbar) \otimes \exp(iH_0t/\hbar)$  is the dynamical map corresponding to the bare system,  $H_0$ .

To obtain the transfer tensors  $T_k$ , and consequently the memory kernels  $\mathcal{K}_k$ , the dynamical maps,  $\mathcal{E}(t)$ , are simulated using path integrals. These dynamical maps propagate the reduced density matrix of the system in the presence of the environment. Suppose that at the initial time the system is in a separable state with the environment in a thermal equilibrium,  $\rho(0) = \tilde{\rho}(0) \otimes \exp(-\beta H_{\text{env}})/Z$ . Then the dynamical map of the system in presence of the environment can be obtained using non-perturbative, numerically exact path integral methods:<sup>18,19</sup>

$$\tilde{\rho}(N\Delta t) = \mathcal{E}(N\Delta t)\tilde{\rho}(0) \quad (9)$$

$$\begin{aligned} \langle s_N^\pm | \mathcal{E}(N\Delta t) | s_0^\pm \rangle &= \sum_{s_1^\pm} \dots \sum_{s_{N-1}^\pm} \langle s_N^\pm | \mathcal{E}_0(\Delta t) | s_{N-1}^\pm \rangle \\ &\times \langle s_{N-1}^\pm | \mathcal{E}_0(\Delta t) | s_{N-2}^\pm \rangle \dots \\ &\times \langle s_1^\pm | \mathcal{E}_0(\Delta t) | s_0^\pm \rangle F[\{s_i^\pm\}] \end{aligned} \quad (10)$$

where  $s_i^\pm$  is the state of the system at  $i$ th time point and  $F[\{s_i^\pm\}]$  is the Feynman-Vernon influence functional<sup>15</sup> along the path  $\{s_i^\pm\}$ . The interactions between different time points caused by environmental effects, which are encoded in the influence functional, are related to the spectral density, Eq. 4, and the bath response function.<sup>43</sup>

With the memory kernels  $\mathcal{K}_j$  in hand, we discretize Eq. 5 to finally get the reduced density matrix at the  $n$ th time-step with the incorporation of loss mechanisms

$$\begin{aligned} \tilde{\rho}_n^{(L)} &= \mathcal{E}_0(\Delta t) \tilde{\rho}_{n-1}^{(L)} + \sum_{j=1}^L \mathcal{K}_j \tilde{\rho}_{n-j}^{(L)} \Delta t^2 \\ &+ \sum_j \left( L_j \tilde{\rho}_{n-1}^{(L)} L_j^\dagger - \frac{1}{2} \{ L_j^\dagger L_j, \tilde{\rho}_{n-1}^{(L)} \} \right) \Delta t. \end{aligned} \quad (11)$$

Now, we are in a position to simulate linear spectra of any open quantum system. A linear spectra is related to the Fourier transform of a system time correlation function of the form:

$$C_{A-B}(t) = \text{Tr} [A(t)B(0)\rho(0)], \quad (12)$$

$$\text{where } \rho(0) = \tilde{\rho}(0) \otimes \frac{e^{-\beta H_{\text{env}}}}{Z_{\text{env}}} \quad (13)$$

and  $A$  and  $B$  are system operators. One can define a time-evolved quantity

$$\rho_B(t) = \text{Tr}_{\text{env}} [\exp(-iHt/\hbar) B \rho(0) \exp(iHt/\hbar)] \quad (14)$$

which can be computed using PILD for an arbitrary environment. Now, the correlation function can be obtained as  $C_{A-B}(t) = \text{Tr}_{\text{sys}} [A \rho_B(t)]$ . The subscripts, sys and env, denote partial trace over system and environment degrees of freedom respectively.

The two specific cases of linear spectra that are studied here are the absorption and the circular dichroism spectra. The absorption spectra is the real part of the Fourier transform of the transition dipole moment auto-correlation function ( $A = B = \mu$ )

$$\sigma_{\text{abs}}(\omega) \propto \text{Re} \left[ \int_0^t e^{i\omega t} C_{\mu-\mu}(t) dt \right] \quad (15)$$

where  $\mu = \sum_j \mu_j$  is the total transition dipole moment constituted by the individual molecular transition dipoles,  $\mu_j$ . For a molecular aggregate, the CD spectrum is defined in terms of the correlation function with  $A = m$  and  $B = \mu$  as<sup>44</sup>

$$\sigma_{\text{CD}}(\omega) \propto \text{Im} \left[ \int_0^t e^{i\omega t} C_{\mu-m}(t) dt \right] \quad (16)$$

where the magnetic moment of the aggregate,  $m \propto \sum_j \vec{r}_j \times \mu_j$  given that the  $j$ th molecule with a transition dipole of  $\mu_j$  is located at  $\vec{r}_j$ . The CD spectrum is instrumental in analysing orientational chirality in molecular aggregates. Using the correlation function-based definitions of the spectra allows for an exact simulation of the lineshape for a particular environment at a particular temperature.

### III. NUMERICAL RESULTS & ANALYSIS

We will explore the spectra of two different classes of systems. The first being that of an excitonic molecular aggregate, which is described by a Frenkel-Holstein Hamiltonian given in Eq. 1. The corresponding system as defined by Eq. 2 has  $N$  bacteriochlorophyll (BChl) molecules of equal monomer excitation energy ( $\epsilon_j = \epsilon$  for all  $j$ ) that interact in a nearest-neighbor fashion ( $h_{j,k} = 0$  for  $|j-k| > 1$ ) in two different geometries, the right-handed helix ( $h_{j,j+1} = 363 \text{ cm}^{-1}$ ) and the right-handed

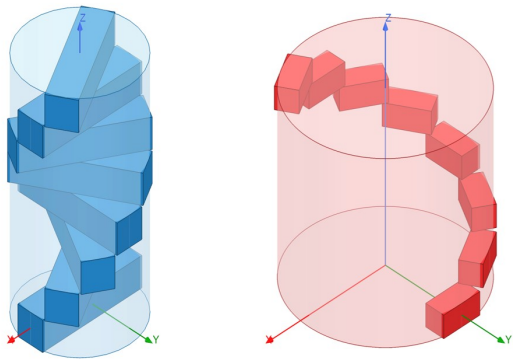


FIG. 1. Geometries of molecular aggregates: Helix (right-handed) (left, blue) and Creeper (right-handed) (right, red)

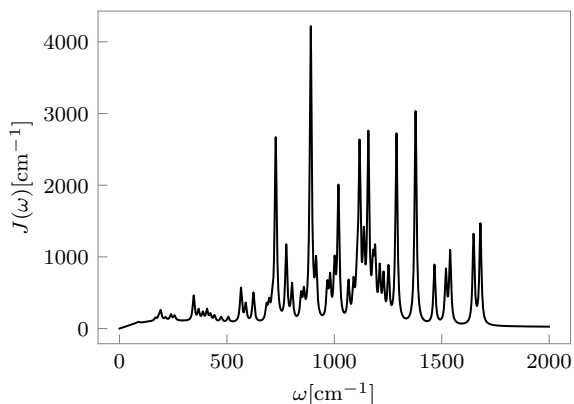


FIG. 2. Spectral density corresponding to a bacteriochlorophyll molecule with reorganization energy of  $327 \text{ cm}^{-1}$ .

creeper ( $h_{j,j+1} = -363 \text{ cm}^{-1}$ ). The consecutive individual molecular transition dipoles of both arrangements are rotated counterclockwise by  $\frac{\pi}{6}$ . For the helix, the molecular centers are all aligned along  $z$ -axis, whereas the displacement vectors for consecutive molecules make an angle of  $\frac{\pi}{4}$  with the  $z$ -axis and the projections of their position vectors in the  $xy$ -plane make an angle of  $\frac{\pi}{6}$  with each other for the creeper geometry. The intermolecular distance for the creeper is 0.79 times that of the helix. Both these arrangements are graphically depicted in Fig. 1.

The vibrations associated with the BChl monomers have been incorporated using the Huang-Rhys factors corresponding to the interaction between 50 of the most strongly coupled vibrations and the excited state of the molecules which have been reported by Rätsep *et al.*<sup>45</sup> These include only relatively rigid molecular vibrations. To make the system more realistic, we have augmented the spectral density using a Brownian bath described by a Drude-Lorentz spectral density with a reorganization energy of  $109 \text{ cm}^{-1}$  and broadened the sharp Huang-Rhys factors by a Lorentzian of width  $10.97 \text{ cm}^{-1}$ . The result-

ant spectral density is shown in Fig. 2. The temperature is set to 300 K.

The second class of systems whose spectra we explore is exciton-polaritonic in nature. The same BChl aggregates that were just described are put inside a cavity. The system can now be written as

$$H_0 = \sum_j \epsilon_j |j\rangle\langle j| + \sum_j h_{j,j+1} (|j\rangle\langle j+1| + |j+1\rangle\langle j|) + \hbar\omega_c |c\rangle\langle c| + \frac{1}{\sqrt{N}} \sum_j s_j (|c\rangle\langle j| + |j\rangle\langle c|), \quad (17)$$

where  $|c\rangle$  is the state with all the molecules in the ground state and the cavity in the excited state,  $\omega_c$  is the frequency of the cavity, and  $s_j$  is the coupling of the  $j$ th monomer to the cavity. Assuming the electric field of the cavity mode to be aligned with transition dipole moment of the first monomer, we take  $s_j = s \cos[(j-1)\frac{\pi}{6}]$  where  $s = 403.28 \text{ cm}^{-1}$  and  $\hbar\omega_c = \epsilon$ . It is also important to note that the cavity is not coupled to a thermal environment.

Both the spectra are governed by correlation functions involving the total transition dipole moment of the aggregate. This is obtained as

$$\mu = \sum_j \vec{\mu}_j (|j\rangle\langle 0| + |0\rangle\langle j|). \quad (18)$$

Notice that the transition dipole moment operator does not involve the cavity.

We will explore the effect of loss from a particular monomer,  $|j\rangle$ , with a decay time constant,  $\tau$ , on the absorption and circular dichroism spectrum in various cases. This can be described by the Lindblad operator,  $L_j = \tau^{-1/2} |0\rangle\langle j|$ . Additionally, in the cases of excitonic-polaritons, the cavities are generally leaky. This loss can be captured by the corresponding Lindblad operator,  $L_c = \tau_c^{-1/2} |0\rangle\langle c|$ . The simulations are done using the path integral Lindblad method<sup>36</sup> with the transfer tensors being generated using the time-evolved matrix product operators (TEMPO) algorithm<sup>23</sup> with multiple baths<sup>46</sup> as implemented in the open-source QuantumDynamics.jl simulation framework.<sup>47</sup> The inclusion of loss through the PILD guarantees certain conserved quantities in the form of sum rules. The area under the linear spectra, being related to the zero time value of correlation functions, is invariant to the loss incorporated in the system.

### A. Spectroscopy of Excitonic Molecular Aggregates

We start by exploring the spectra of the excitonic molecular aggregates under losses with different decay times. Consider a BChl dimer in the creeper and the helix formations. In Fig. 3, we show the absorption and CD spectra for the system with decay times,  $\tau = 25 \text{ fs}$ ,  $50 \text{ fs}$  and  $75 \text{ fs}$  along with that of the loss-less dimer (in solid curve). The profile of the absorption peak of the

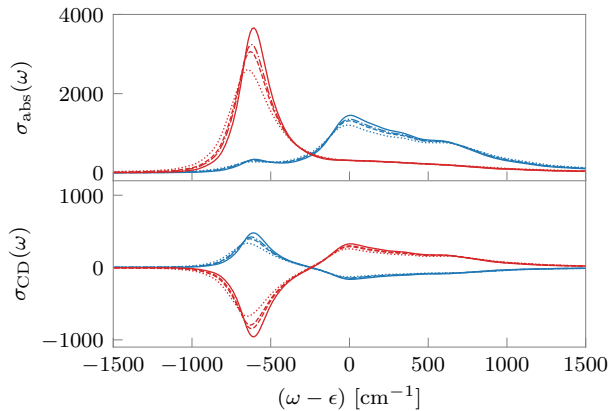
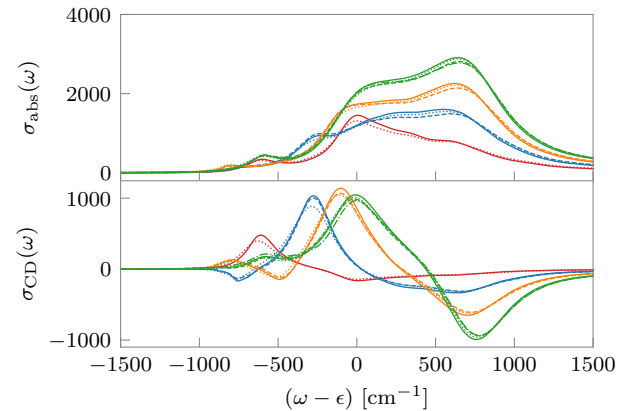


FIG. 3. Absorption and CD spectra of BChl dimers in Helix (H-aggregate) (Blue) and Creeper (J-aggregate) (Red) geometries for different decay constants  $\tau = 25$  fs (dotted), 50 fs (dashed), 75 fs (dash-dot), and the loss-less case (solid).

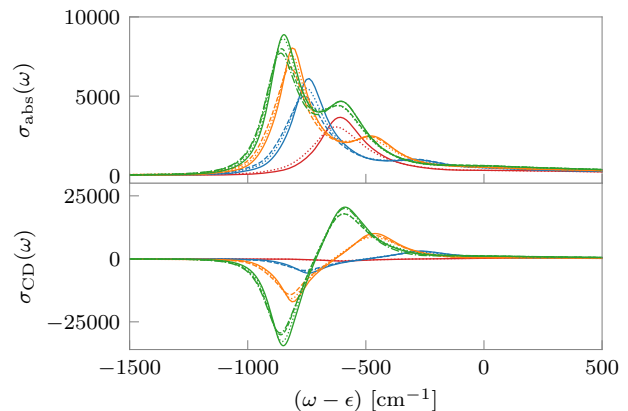
helix is significantly more structured and broader than that of the creeper. It is usual for H-aggregates to have more broadened spectra compared to the J-aggregates when coupled with structured vibrational bath.<sup>54</sup> The CD spectrum shows a positive first and a negative second Cotton feature for the helix geometry which is opposite to that of the creeper geometry despite both geometries being right-handed. It is notable that, while the two expected peaks corresponding to the two bright excitonic states for a noncoplanar dimer are not easily discernible from the absorption spectrum (especially for the creeper), it is possible to clearly locate them from the CD spectrum.

In Fig. 3, it is clearly seen that though both the helix and the creeper geometries have the same absolute chirality, the CD spectra have different Cotton effects. This is in apparent contradiction of the often-used exciton-chirality (EC) rule, which uniquely maps the sign of the lowest-energy Cotton couplet to the absolute chirality of the aggregate.<sup>48–50</sup> However, Swathi *et al.*<sup>51</sup> have shown that, consistent with our results here, the EC mapping is reversed between the H- and J- dimers.

On applying the different losses, the spectral feature of the dimer broaden and become less intense. Notice that the relative decrease in the intensity of the primary absorption peak with respect to the loss-less case is more for the creeper than for the helix. This broadening is also accompanied by an increasing red shift of the spectra. (This is also seen in the absence of the dissipative environment as demonstrated in Appendix A.) The red shift of the  $\omega < \epsilon$  peak seems to be higher than that of the  $\omega \geq \epsilon$  peak. In addition, the relative magnitude of attenuation of the peak height of the helix is much smaller than that of the creeper. These observations also extend to the CD spectrum where the shift and attenuation due to loss mechanisms are more prominent for the sharper peaks (or troughs).



(a) Helix geometry



(b) Creeper geometry

FIG. 4. Absorption and CD spectra of BChl Dimer (Red), Trimer (Blue), Tetramer (Orange) and Pentamer (Green) for decay constant  $\tau = 50$  fs at monomer 1 (dotted), monomer 2 (dashed), monomer 3 (dash-dot) and the loss-less cases (solid).

From the dimer as a representative case, we proceed to investigate the effect of exciton system size vis-à-vis decay time  $\tau$  in Fig. 4 (a) and (b). We look at the dimer, trimer, tetramer, and pentamer with the same nearest-neighbor intermolecular couplings. Losses with a decay time of  $\tau = 50$  fs are applied to each of the unique sites in the aggregate. For the trimer and tetramer, monomers 1 and 2 constitute the two distinct sites of decay while for the pentamer, monomer 3 is an additional unique site. While we observe the expected red shift in the absorption spectra for the J-creepers (Fig. 4 (b)) for all system sizes, there is an increasing blue shift for the trimer H-helices and beyond (Fig. 4 (a)). The impact of a loss on a single site is seen to decrease with increasing system size. Moreover, decay at the central monomer is more effective in attenuating the intensity of spectrum than the decay at other site owing to symmetries of the system.

The CD spectra shown in Fig. 4 (a) and (b) enables identification of various peaks obscured in the absorp-

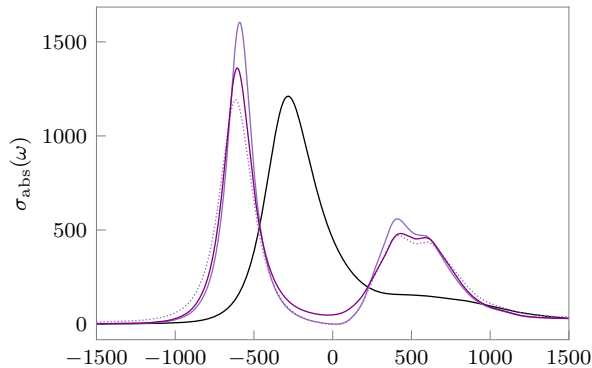
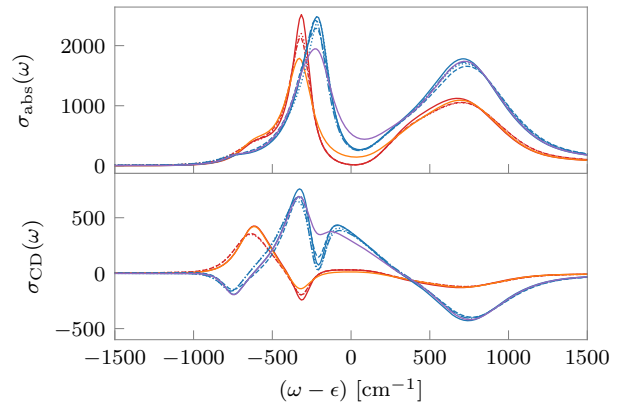


FIG. 5. Absorption spectrum of BChl Monomer with (Purple) and without (Black) an Optical Cavity for decay constant  $\tau = 50$  fs at monomer (dotted), cavity (solid; darker shade) and the loss-less case (solid; lighter shade).

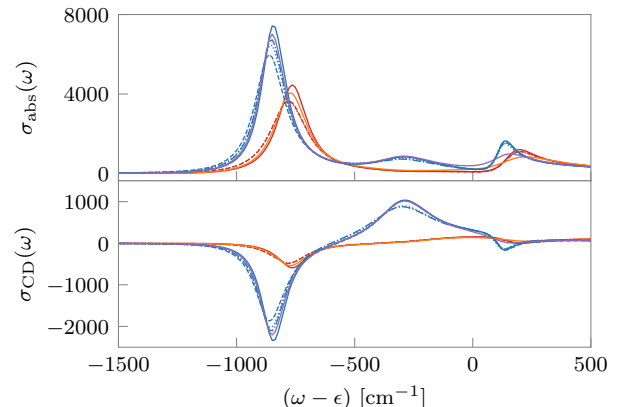
tion spectrum. For the J-creepers, the sign of the first peak is consistently seen to be negative at all sizes of the aggregates. However, it is interesting that all the H-helices do not show the same sign of the first peak of the CD spectra. For the case of the helix trimer, one sees the initial peak become negative instead of the positive peak seen in the other helices. This further shows that the EC mapping between the CD spectra and the corresponding geometry is even more tenuous. Earlier we had discussed the inconsistency between a helix and creeper dimer. Now we note the inconsistency between helices of different sizes. However, this pattern can be explained for the bare system through a calculation of the rotational strengths of each of the excitonic states as outlined in Appendix B. Also, as seen in the case of the isolated pentamer, for both the creeper and the helix, there are only three states that are CD active.

## B. Spectroscopy of Excitonic-Polaritonic Systems

As a second class of systems of interest, we consider excitonic systems coupled with a plane-polarized cavity mode. In Fig. 5, we see how upon coupling to the cavity mode, a monomer absorption peak splits into two polaritonic peaks corresponding to the lower energy “Lower Polariton” and higher energy “Upper Polariton” which are the two eigenstates of Eq. 17. In absence of any loss, the upper polariton shows a broader line-shape, which correlates with a lower lifetime in comparison to the lower polariton. We notice that similar to the excitonic systems, the decrease in intensity and broadening of peaks on the inclusion of loss mechanisms are not equal. It is more for the lower polariton than the upper polariton. This difference, while relatively minor when the cavity is lossy, becomes clearly noticeable when the loss is on the monomer. This is entirely due to interaction of the environment with the different polaritons (Appendix A).



(a) Helix geometry



(b) Creeper geometry

FIG. 6. Absorption and CD spectra of BChl Dimer (Red) and Trimer (Blue) in an optical cavity for decay constant  $\tau = 50$  fs at monomer 1 (dotted), monomer 2 (dashed), monomer 3 (dash-dot), cavity (dimer: orange, trimer: purple) and the loss-less cases (solid).

However, unlike the excitons, where loss mechanisms always led to a red shift in the absorption spectrum, the lower polariton  $|L\rangle$  experiences a red shift while the upper polariton,  $|U\rangle$  a blue shift. This effective expansion of the polaritonic spectrum is opposite to the compression observed in the absence of the dissipative environment as demonstrated in Appendix A. Interestingly, a similar effect has been noticed using non-Hermitian systems to model the dissipation and the so-called  $P(E)$  theory.<sup>52</sup> Here we can quantify the non-perturbative effects of the thermal environment in a numerically exact manner. Thus, while the lower polariton is energetically stabilized by the external loss, its lifetime decreases more prominently than the upper polariton.

Finally, in Fig. 6 (a) and (b), we demonstrate the absorption and CD spectra for BChl dimer and trimer coupled to a cavity mode. While a polaritonic system described by the Holstein-Tavis-Cummings model has only two bright states,<sup>53</sup> here we have more. This apparent

discrepancy stems from the Holstein-Tavis-Cummings model ignoring the intermolecular coupling. We notice in both geometries that the effect of a loss at the cavity is qualitatively different from that at the monomers. For the helix geometry, the lowest and highest energy CD peaks seem to remain relatively unaffected by a cavity loss. The intermediate peaks are all highly damped. The effect seems to be reversed for the creeper geometry (Fig. 6 (b)). Thus, there is a more marked decrease in lifetime of particular polaritons due to the loss mechanisms. Additionally, it is interesting that the first CD couplet resembles the excitonic system thereby aiding in identification of the geometry of the aggregate. The CD spectra actually provides a way to identify the dark states as the peaks (or troughs) which are least affected by loss at cavity because of the small contribution of cavity mode to these states.

The interpretation of the CD spectra, the changes that happen in them due to loss, and correlating it with structure of the polaritonic system is a highly nuanced endeavor. This will be explored in the future in greater detail.

#### IV. CONCLUSION

In this paper, we present a numerically rigorous study of the impact of empirically described loss mechanisms on two different linear spectra, absorption spectra and circular dichroism spectra, of condensed phase systems using the recently developed path integral Lindblad dynamics method. Empirical loss mechanisms are often incorporated using non-Hermitian descriptions which make the time-evolution non-unitary. This has spurious effects on the spectra. PILD ensures that the dynamical maps are unitary and consequently avoids such spurious effects. An additional benefit of PILD is that one can get the effect of these loss mechanisms at no extra cost, while maintaining the accuracy of the method and the rigor of accounting for the effects of the thermal dissipative environment. One of the consequences of the accuracy of these simulations is that the area under the spectra are invariant under changing the time-scale of the losses.

Intuitively, one might think that the effect of loss is the broadening of the spectrum. This is indeed the primary effect. However, the details are much more complex. Different peaks get broadened in different ways. The empirical loss also “interacts” with the dissipative environment to have more complex and apparently unpredictable amounts of loss. Additionally, this broadening can also be accompanied by a shift of the peak. We demonstrate these complexities through various examples.

We consider the absorption and the CD spectra of chiral excitonic aggregates and chiral polaritonic aggregates formed by these systems inside a nonchiral, plane-polarized cavity. The numerically exact spectra of the excitonic aggregates are already quite complicated. We

show that different peaks get attenuated at different rates. The magnitude of the lossy site to the particular exciton, while an important consideration, is not the only factor which determines the amount by which the peak would get attenuated. There are complex interactions mediated by the environment which couples different excitons together. Additionally, we see that the helix aggregate with primarily H-type interactions have far broader peaks than the creeper aggregate with J-like interactions. This greater structure has typically been attributed to exciton-phononic bands<sup>54</sup> for simple cases.

The presence of the cavity adds to the complexity of the problem. The excitonic absorption peaks get split into multiple polaritonic peaks. We report probably the first numerically exact path integral simulations of CD spectra of chiral aggregates in cavity. The chirality of the different polaritonic peaks interacts in unexpected manners. For a monomer or a dimer for instance, the upper polariton gets attenuated significantly less than the lower polariton.

All these complexities and subtleties necessitate rigorous simulation frameworks for predicting the spectra in these open quantum systems. We provide the first exploration of such effects by using the rigorous and fully quantum mechanical PILD framework based on TEMPO QuAPI calculations. The ability to understand and predict the spectra provides a powerful handle on the properties of these complex aggregates. This would be a topic of exploration and study in the future. Further these numerically exact methods will be used to elaborate the routes of transport and their relative efficiencies in a future work.

#### Appendix A: Spectra of lossy systems without vibrational decohering environments

To understand the changes better, we demonstrate the impact of the loss analytically on the spectra of a linear (co-planar) excitonic dimer and a monomer interacting with a cavity mode without any thermal environment. This can be done analytically and enables separation of impact caused solely by the loss versus that caused through the mediation of the environment.

Consider first the excitonic dimer without the dissipative environment as defined in Eq. 2 with equal monomer excitation energy  $\epsilon$  and intermonomer coupling as  $h_{12}$  ( $= h_{21}$ ). As in the cases described earlier, there is a loss with a time-scale of  $\tau$  on the second monomer given by  $L_2 = \tau^{-1/2} |0\rangle\langle 2|$ . For simplicity of analysis, we assume that the decay timescale is relatively weak,  $\tau > \frac{\hbar}{4h_{12}}$ . This would typically be the case because the electronic couplings between the monomers would be stronger than the time-scales of a loss process. The transition dipole moment operator is defined in Eq. 18 with equal magnitudes  $\mu$  for each monomer. The absorption spectrum can

now be calculated using the relation 15 to get:

$$\sigma_{\text{abs}}^{(2)}(\omega) \propto \mu^2 \frac{b}{a} \left[ \frac{a + h_{12}/\hbar}{(\omega - a - \epsilon/\hbar)^2 + b^2} + \frac{a - h_{12}/\hbar}{(\omega + a - \epsilon/\hbar)^2 + b^2} \right] \quad (\text{A1})$$

where for  $a = \sqrt{\frac{h_{12}^2}{\hbar^2} - \frac{1}{16\tau^2}}$  and  $b = \frac{1}{4\tau}$ . Notice that this is a sum of two Lorentzians centered at  $\omega_0 = a + \epsilon/\hbar$  and  $\omega_1 = -a + \epsilon/\hbar$  respectively. If  $\tau \gg \frac{\hbar}{4h_{12}}$ , then the

intensity of the peak at  $\omega_1$  would be very small and can be neglected. Consequently on decreasing  $\tau$  (i.e., a stronger decay), the dominant peak at  $\omega_0$  shows a red-shift owing to the decrease in the value of  $a$ .

Similarly, for a monomer-cavity system defined with Eq. 17 with the cavity resonant with monomer excitation energy,  $\hbar\omega_c = \epsilon$ , cavity coupling  $s$  and transition dipole moment as defined in Eq. 18 with magnitude  $\mu$ , we consider the two cases with the loss on the cavity  $L_c = \tau^{-1/2} |0\rangle\langle c|$  and a loss on the monomer  $L_1 = \tau^{-1/2} |0\rangle\langle 1|$ . The corresponding absorption spectra for the loss on the cavity and the monomer are:

$$\sigma_{\text{abs}}^{(c)}(\omega) \propto \mu^2 \frac{b}{2a'} \left[ \frac{2a' - \omega + \epsilon/\hbar}{(\omega - a' - \epsilon/\hbar)^2 + b^2} + \frac{2a' + \omega - \epsilon/\hbar}{(\omega + a' - \epsilon/\hbar)^2 + b^2} \right] \quad (\text{A2})$$

$$\sigma_{\text{abs}}^{(1)}(\omega) \propto \mu^2 \frac{b}{2a'} \left[ \frac{\omega - \epsilon/\hbar}{(\omega - a' - \epsilon/\hbar)^2 + b^2} - \frac{\omega - \epsilon/\hbar}{(\omega + a' - \epsilon/\hbar)^2 + b^2} \right] \quad (\text{A3})$$

Here,  $a' = \sqrt{\frac{s^2}{\hbar^2} - \frac{1}{16\tau^2}}$ , which is the same as  $a$  but with  $h_{12}$  replaced by  $s$  while the symbol in superscript parenthesis denotes the site of loss.

We can now see from the relation A2 for the loss on cavity that instead of shifting in the same direction, the lower energy polariton shifts blue, whereas the higher energy polariton shifts red. This is exactly opposite to what we saw in presence of the dissipative media (Fig. 5). However with relation A3 for the loss on monomer, there is no conspicuous shift in the spectrum. It is also to be noted that the lineshape for the two polaritonic peaks are symmetrical despite the inclusion of loss at any site.

## Appendix B: Rotatory strengths for peaks of excitonic aggregates

Here we discuss the rotatory matrix and the strengths for bare excitonic and polaritonic aggregates in absence of thermal dissipative environments. Consider a general aggregate, either excitonic or polaritonic, described by a Hamiltonian,  $\hat{H}_0$ , with  $N$  molecules located at  $\vec{\mathbf{r}}_j$  with transition dipoles  $\vec{\mu}_j$ . The cross correlation function between the transition dipole moment and the magnetic moment can be refactored as follows:

$$\sigma_{\text{CD}}(\omega) = \text{Re} \int_0^\infty \sum_{ij} R_{ji} I_{ij}(t) \exp(i\omega t) \quad (\text{B1})$$

where:

$$R_{ji} = -\sqrt{\epsilon_i \epsilon_j} (\vec{\mathbf{r}}_j - \vec{\mathbf{r}}_i) \cdot (\vec{\mu}_i \times \vec{\mu}_j) \quad (\text{B2})$$

$$I_{ij}(t) = e^{iE_g t/\hbar} \text{Tr}_{\text{env}} \left( \langle j | e^{-iHt/\hbar} | i \rangle \right) \quad (\text{B3})$$

The rotatory strength matrix is  $R$  and  $I(t)$  is the lineshape function. Now, this is defined in the molecular basis. We want the strengths corresponding to the different eigenstates of the system Hamiltonian  $\hat{H}_0$ ,  $|e_j\rangle$ . These states,  $|e_j\rangle$ , correspond to excitons in the molecular aggregates and polaritons in presence of cavities. It is possible to transform the spectrum from a molecular basis to the eigenstate basis:

$$\begin{aligned} \sigma_{\text{CD}}(\omega) &= \text{Re} \int_0^\infty \text{Tr} (RI(t)) \exp(i\omega t) \quad (\text{B4}) \\ &= \text{Re} \int_0^\infty \sum_{ij} \langle e_i | R | e_j \rangle \langle e_j | I(t) | e_i \rangle \exp(i\omega t) \quad (\text{B5}) \end{aligned}$$

For an isolated system in absence of dissipative environment, the transformation is simple. The lineshape function matrix is diagonal in the  $|e_j\rangle$  basis. It is the presence of the dissipative environment that couples the different eigenstates. Consequently, the peak heights for an isolated system are proportional to the matrix element of the rotatory strength matrix corresponding to the particular eigenstate,  $\langle e_j | R | e_j \rangle$ .

$$\sigma_{\text{CD}}(\omega) = \sum_i \langle e_i | R | e_i \rangle \delta(\omega - E_i - E_g). \quad (\text{B6})$$

In Tables I and II, we list the locations and the heights of the CD peaks for different sized nearest neighbor creeper and helix aggregates with  $|h_{12}| = 363.0 \text{ cm}^{-1}$ . Notice that in absence of the thermal environment, the peak heights are exactly reversed between the helix and the creeper. The locations are the same. With the size of the aggregate, the height of the peak increases in case of the creeper. However, there is no apparent pattern

Dimer		Trimer		Tetramer		Pentamer	
$\omega'$ (cm <sup>-1</sup> )	$\sigma_{CD}(\omega)$						
-363.0	-0.5	-513.36	-1.57	-587.35	-3.19	-628.73	-5.20
+363.0	+0.5	0.0	+1.73	-224.35	+3.41	-363.0	+5.10
		+513.36	-0.16	+224.35	-0.31	0.0	0.0
				+587.35	+0.09	+363.0	+0.10
						+628.73	0.0

TABLE I. CD peak heights for isolated creeper aggregate as a function of aggregate size. ( $\omega' = \omega - \epsilon$ )

Dimer		Trimer		Tetramer		Pentamer	
$\omega'$ (cm <sup>-1</sup> )	$\sigma_{CD}(\omega)$						
-363.0	+0.5	-513.36	-0.16	-587.35	+0.09	-628.73	0.0
+363.0	-0.5	0.0	+1.73	-224.35	-0.31	-363.0	+0.10
		+513.36	-1.57	+224.35	+3.41	0.0	0.0
				+587.35	-3.19	+363.0	+5.10
						+628.73	-5.20

TABLE II. CD peak heights for isolated helix aggregate as a function of aggregate size. ( $\omega' = \omega - \epsilon$ )

for the helix. With regards to the sign of the first peak, notice that just as seen in presence of the environment, irrespective of the aggregate size, the creeper has a negative peak first. We see that the sign of the first peak of the helix keeps alternating between a positive and a negative sign. This apparently simple pattern for helices is further complicated by the fact that some times, like in the case of a pentamer, the first peak has zero intensity. In that case, effectively, the first peak that is symmetry allowed would be positive again. These patterns are consistent with the spectra calculated in the presence of the solvent.

- <sup>1</sup>S. R. White, "Density matrix formulation for quantum renormalization groups," *Physical Review Letters* **69**, 2863–2866 (1992).
- <sup>2</sup>U. Schollwöck, "The density-matrix renormalization group," *Reviews of Modern Physics* **77**, 259–315 (2005).
- <sup>3</sup>U. Schollwöck, "The density-matrix renormalization group in the age of matrix product states," *Annals of Physics* **326**, 96–192 (2011).
- <sup>4</sup>S. Paeckel, T. Köhler, A. Swoboda, S. R. Manmana, U. Schollwöck, and C. Hubig, "Time-evolution methods for matrix-product states," *Annals of Physics* **411**, 167998 (2019).
- <sup>5</sup>H.-D. Meyer, U. Manthe, and L. Cederbaum, "The multi-configurational time-dependent Hartree approach," *Chemical Physics Letters* **165**, 73–78 (1990).
- <sup>6</sup>H. Wang and M. Thoss, "Multilayer formulation of the multi-configuration time-dependent Hartree theory," *The Journal of Chemical Physics* **119**, 1289–1299 (2003).
- <sup>7</sup>H. Wang, "Multilayer Multiconfiguration Time-Dependent Hartree Theory," *The Journal of Physical Chemistry A* **119**, 7951–7965 (2015).
- <sup>8</sup>F. Bloch, "Generalized Theory of Relaxation," *Physical Review* **105**, 1206–1222 (1957).
- <sup>9</sup>A. G. Redfield, "On the Theory of Relaxation Processes," *IBM J. Res. Dev.* **1**, 19–31 (1957).
- <sup>10</sup>G. Lindblad, "On the generators of quantum dynamical semigroups," *Communications in Mathematical Physics* **48**, 119–130 (1976).
- <sup>11</sup>V. Gorini, A. Kossakowski, and E. C. G. Sudarshan, "Completely positive dynamical semigroups of N-level systems," *Journal of Mathematical Physics* **17**, 821–825 (1976).
- <sup>12</sup>J. C. Tully, "Molecular dynamics with electronic transitions," *The Journal of Chemical Physics* **93**, 1061–1071 (1990).

- <sup>13</sup>J. C. Tully and R. K. Preston, "Trajectory Surface Hopping Approach to Nonadiabatic Molecular Collisions: The Reaction of H<sup>+</sup> with D<sub>2</sub>," *The Journal of Chemical Physics* **55**, 562–572 (2003).
- <sup>14</sup>R. P. Feynman, A. R. Hibbs, and D. F. Styer, *Quantum Mechanics and Path Integrals*, emended ed. (Dover Publications, Mineola, N.Y., 2010).
- <sup>15</sup>R. P. Feynman and F. L. Vernon, "The theory of a general quantum system interacting with a linear dissipative system," *Annals of Physics* **24**, 118–173 (1963).
- <sup>16</sup>Y. Tanimura and P. G. Wolynes, "Quantum and classical Fokker-Planck equations for a Gaussian-Markovian noise bath," *Physical Review A* **43**, 4131–4142 (1991).
- <sup>17</sup>Y. Tanimura, "Numerically "exact" approach to open quantum dynamics: The hierarchical equations of motion (HEOM)," *The Journal of Chemical Physics* **153**, 20901 (2020).
- <sup>18</sup>N. Makri and D. E. Makarov, "Tensor propagator for iterative quantum time evolution of reduced density matrices. I. Theory," *The Journal of Chemical Physics* **102**, 4600–4610 (1995).
- <sup>19</sup>N. Makri and D. E. Makarov, "Tensor propagator for iterative quantum time evolution of reduced density matrices. II. Numerical methodology," *The Journal of Chemical Physics* **102**, 4611–4618 (1995).
- <sup>20</sup>J. Cerrillo and J. Cao, "Non-Markovian Dynamical Maps: Numerical Processing of Open Quantum Trajectories," *Physical Review Letters* **112**, 110401 (2014).
- <sup>21</sup>H. Rahman and U. Kleinekathöfer, "Chebyshev hierarchical equations of motion for systems with arbitrary spectral densities and temperatures," *The Journal of Chemical Physics* **150**, 244104 (2019).
- <sup>22</sup>M. Xu, Y. Yan, Q. Shi, J. Ankerhold, and J. T. Stockburger, "Taming Quantum Noise for Efficient Low Temperature Simulations of Open Quantum Systems," *Physical Review Letters* **129**, 230601 (2022).
- <sup>23</sup>A. Strathearn, P. Kirton, D. Kilda, J. Keeling, and B. W. Lovett, "Efficient non-Markovian quantum dynamics using time-evolving matrix product operators," *Nature Communications* **9**, 3322 (2018).
- <sup>24</sup>M. R. Jørgensen and F. A. Pollock, "Exploiting the Causal Tensor Network Structure of Quantum Processes to Efficiently Simulate Non-Markovian Path Integrals," *Physical Review Letters* **123**, 240602 (2019).
- <sup>25</sup>N. Makri, "Small matrix disentanglement of the path integral: Overcoming the exponential tensor scaling with memory length," *The Journal of Chemical Physics* **152**, 41104 (2020).
- <sup>26</sup>A. Bose and P. L. Walters, "A multisite decomposition of the

- tensor network path integrals,” *The Journal of Chemical Physics* **156**, 024101 (2022).
- <sup>27</sup>A. Bose and P. L. Walters, “Impact of Solvent on State-to-State Population Transport in Multistate Systems Using Coherences,” *Journal of Chemical Theory and Computation* **19**, 4828–4836 (2023).
- <sup>28</sup>A. Bose, “Quantum correlation functions through tensor network path integral,” *The Journal of Chemical Physics* **159**, 214110 (2023).
- <sup>29</sup>Y. Yan, M. Xu, T. Li, and Q. Shi, “Efficient propagation of the hierarchical equations of motion using the Tucker and hierarchical Tucker tensors,” *The Journal of Chemical Physics* **154**, 194104 (2021).
- <sup>30</sup>S. Kundu, R. Dani, and N. Makri, “B800-to-B850 relaxation of excitation energy in bacterial light harvesting: All-state, all-mode path integral simulations,” *The Journal of Chemical Physics* **157**, 015101 (2022), <https://doi.org/10.1063/5.0093828>.
- <sup>31</sup>A. Bose and P. L. Walters, “Tensor Network Path Integral Study of Dynamics in B850 LH2 Ring with Atomistically Derived Vibrations,” *Journal of Chemical Theory and Computation* **18**, 4095–4108 (2022).
- <sup>32</sup>A. Bose and P. L. Walters, “Impact of Spatial Inhomogeneity on Excitation Energy Transport in the Fenna–Matthews–Olson Complex,” *The Journal of Physical Chemistry B* **127**, 7663–7673 (2023).
- <sup>33</sup>P. Huo and D. F. Coker, “Communication: Partial linearized density matrix dynamics for dissipative, non-adiabatic quantum evolution,” *The Journal of Chemical Physics* **135**, 201101 (2011).
- <sup>34</sup>J. Provazza, F. Segatta, M. Garavelli, and D. F. Coker, “Semi-classical Path Integral Calculation of Nonlinear Optical Spectroscopy,” *Journal of Chemical Theory and Computation* **14**, 856–866 (2018).
- <sup>35</sup>M. E. Mondal, E. R. Koessler, J. Provazza, A. N. Vamivakas, S. T. Cundiff, T. D. Krauss, and P. Huo, “Quantum dynamics simulations of the 2D spectroscopy for exciton polaritons,” *The Journal of Chemical Physics* **159**, 094102 (2023).
- <sup>36</sup>A. Bose, “Incorporation of Empirical Gain and Loss Mechanisms in Open Quantum Systems through Path Integral Lindblad Dynamics,” *The Journal of Physical Chemistry Letters* **15**, 3363–3368 (2024).
- <sup>37</sup>C. Olbrich, J. Strümpfer, K. Schulten, and U. Kleinekathöfer, “Theory and Simulation of the Environmental Effects on FMO Electronic Transitions,” *The Journal of Physical Chemistry Letters* **2**, 1771–1776 (2011).
- <sup>38</sup>S. Maity, B. M. Bold, J. D. Prajapati, M. Sokolov, T. Kubař, M. Elstner, and U. Kleinekathöfer, “DFTB/MM Molecular Dynamics Simulations of the FMO Light-Harvesting Complex,” *The Journal of Physical Chemistry Letters* **11**, 8660–8667 (2020).
- <sup>39</sup>S. Nakajima, “On Quantum Theory of Transport Phenomena,” *Progress of Theoretical Physics* **20**, 948–959 (1958).
- <sup>40</sup>R. Zwanzig, “Ensemble Method in the Theory of Irreversibility,” *The Journal of Chemical Physics* **33**, 1338–1341 (1960).
- <sup>41</sup>E. Mulvihill, A. Schubert, X. Sun, B. D. Dunietz, and E. Geva, “A modified approach for simulating electronically nonadiabatic dynamics via the generalized quantum master equation,” *The Journal of Chemical Physics* **150**, 034101 (2019).
- <sup>42</sup>E. Mulvihill and E. Geva, “A Road Map to Various Pathways for Calculating the Memory Kernel of the Generalized Quantum Master Equation,” *The Journal of Physical Chemistry B* **125**, 9834–9852 (2021).
- <sup>43</sup>A. Bose, “Zero-cost corrections to influence functional coefficients from bath response functions,” *The Journal of Chemical Physics* **157**, 054107 (2022).
- <sup>44</sup>L. Cupellini, F. Lipparini, and J. Cao, “Absorption and Circular Dichroism Spectra of Molecular Aggregates With the Full Cumulant Expansion,” *The Journal of Physical Chemistry B* **124**, 8610–8617 (2020).
- <sup>45</sup>M. Rätsep, Z.-L. Cai, J. R. Reimers, and A. Freiberg, “Demonstration and interpretation of significant asymmetry in the low-resolution and high-resolution Qy fluorescence and absorption spectra of bacteriochlorophyll a,” *The Journal of Chemical Physics* **134**, 24506 (2011).
- <sup>46</sup>A. Bose and P. L. Walters, “A tensor network representation of path integrals: Implementation and analysis,” arXiv pre-print server arXiv:2106.12523 (2021), [arxiv:2106.12523](https://arxiv.org/abs/2106.12523).
- <sup>47</sup>A. Bose, “QuantumDynamics.jl: A modular approach to simulations of dynamics of open quantum systems,” *The Journal of Chemical Physics* **158**, 204113 (2023).
- <sup>48</sup>N. Harada, S.-M. L. Chen, and K. Nakanishi, “Quantitative definition of exciton chirality and the distant effect in the exciton chirality method,” *Journal of the American Chemical Society* **97**, 5345–5352 (1975), <https://doi.org/10.1021/ja00852a005>.
- <sup>49</sup>N. Harada, K. Nakanishi, and N. Berova, “Electronic cd exciton chirality method: Principles and applications,” in *Comprehensive Chiroptical Spectroscopy* (John Wiley & Sons, Ltd, 2012) Chap. 4, pp. 115–166, <https://onlinelibrary.wiley.com/doi/pdf/10.1002/9781118120392.ch4>.
- <sup>50</sup>N. Harada and K. Nakanishi, “Optical rotatory power of the benzoate group,” *Journal of the American Chemical Society* **90**, 7351–7352 (1968).
- <sup>51</sup>K. Swathi, C. Sissa, A. Painelli, and K. George Thomas, “Supramolecular chirality: a caveat in assigning the handedness of chiral aggregates,” *Chem. Commun.* **56**, 8281–8284 (2020).
- <sup>52</sup>K. S. U. Kansanen, J. J. Toppari, and T. T. Heikkilä, “Polariton response in the presence of Brownian dissipation from molecular vibrations,” *The Journal of Chemical Physics* **154**, 044108 (2021).
- <sup>53</sup>F. Herrera and F. C. Spano, “Cavity-controlled chemistry in molecular ensembles,” *Phys. Rev. Lett.* **116**, 238301 (2016).
- <sup>54</sup>N. J. Hestand and F. C. Spano, “Expanded theory of h- and j-molecular aggregates: The effects of vibronic coupling and intermolecular charge transfer,” *Chemical Reviews* **118**, 7069–7163 (2018), pMID: 29664617, <https://doi.org/10.1021/acs.chemrev.7b00581>.